NASA TECHNICAL MEMORANDUM

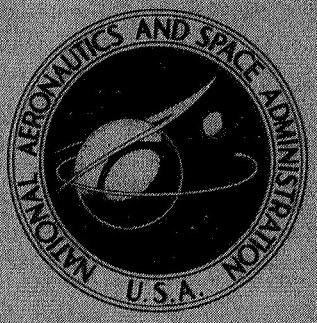

NASA TM X-1662

NASA TM X-1662

EFFECT OF A SIMULATED WING ON THE PRESSURE-DRAG COEFFICIENTS OF VARIOUS 15° BOATTAILS AT MACH NUMBERS FROM 0.56 TO 1.00

by George D. Shrewsbury

Lewis Research Center

Cleveland, Ohio

NATIONAL AERONAUTICS AND SPACE ADMINISTRATION • WASHINGTON, D. C. • OCTOBER 1968

NASA TM X-1662

EFFECT OF A SIMULATED WING ON THE PRESSURE-DRAG COEFFICIENTS OF VARIOUS 15° BOATTAILS AT MACH NUMBERS FROM 0.56 TO 1.00

By George D. Shrewsbury

Lewis Research Center
Cleveland, Ohio

NATIONAL AERONAUTICS AND SPACE ADMINISTRATION

For sale by the Clearinghouse for Federal Scientific and Technical Information
Springfield, Virginia 22151 – CFSTI price $3.00

ABSTRACT

A 10.16-centimeter-diameter-cylindrical-nacelle model was tested in the Lewis 8- by 6-foot supersonic wind tunnel with 15°-conical boattails having radii of curvature of 0-, 0.5-, and 1.0-nacelle diameters at their juncture with the nacelle. The conical nose of the nacelle was closed, and the jet was simulated with a cylindrical surface. The afterbodies were tested with the nozzle exit extended 0.866-, 1.116-, and 1.366-nacelle diameters downstream of a small trapezoidal-wing trailing edge. Data were obtained over a Mach number range from 0.56 to 1.00 at angles of attack from 0° to 6°.

EFFECT OF A SIMULATED WING ON THE PRESSURE-DRAG COEFFICIENTS OF VARIOUS 15° BOATTAILS AT MACH NUMBERS FROM 0.56 TO 1.00

by George D. Shrewsbury

Lewis Research Center

SUMMARY

A 10.16-centimeter-diameter-cylindrical-nacelle model was tested in the Lewis 8- by 6-foot supersonic wind tunnel with 15°-conical boattails having radii of curvature of 0-, 0.5-, and 1.0-nacelle diameters at their juncture with the nacelle. The conical nose of the nacelle was closed, and the jet was simulated with a cylindrical surface. The afterbodies were tested with the nozzle exit extended 0.866-, 1.116-, and 1.366-nacelle diameters downstream of a small trapezoidal-wing trailing edge. Data were obtained over a Mach number range from 0.56 to 1.00 at angles of attack from 0° to 6°.

When compared to isolated boattail data, the presence of the wing flow field with an extension ratio of 0.866 reduced the axial-force coefficients over the entire range of variables tested. The presence of the simulated wing also reduced the effects of angle of attack, especially at the lower subsonic Mach numbers. In general, increasing the boattail-juncture radius of curvature decreases the axial-force coefficient for afterbodies under the influence of a simulated wing with an extension ratio of 0.866. Increasing the nozzle-extension ratio increases the axial-force coefficient of a boattail with a radius of curvature of 0.5-model diameters.

INTRODUCTION

As part of a broad program in airbreathing propulsion, the Lewis Research Center is evaluating various exhaust-nozzle concepts. Supersonic aircraft designed for cruise at Mach numbers up to 3.0 operate over a range of nozzle pressure ratios from approximately 2.0 to 30.0. Nacelles utilizing a variable flap ejector nozzle are normally cylindrical at supersonic cruise but become boattailed at lower Mach numbers as nozzle expansion ratio decreases. The drag incurred by boattailing the nacelle afterbody can be a significant portion of the propulsion system net thrust, especially at subsonic cruise

where the engine is operating at a reduced-power setting.

Drag characteristics of various isolated nacelle afterbodies are reported in references 1 to 3. References 1 and 2 demonstrated the importance of smoothing the boattail juncture with the nacelle with a small radius of curvature.

With an engine-nacelle installation typical for a supersonic-cruise aircraft, the afterbody may be close to the lower surface of a large wing and may extend a short distance downstream of the wing trailing edge. Transonic-wind-tunnel model tests of this installation effect are difficult, however, because of blockage limitations and tunnel-wall-interference effects. If a complete aircraft model is used, the model scale must be small; and, hence, the simulated nacelles are smaller than desired. An alternate approach may be to utilize fairly large nacelle models but only a portion of the wing and airframe. With the latter approach, additional study is required to determine how much of the airframe is necessary to duplicate the major influences of the installation effects. In the present study, a relatively small trapezoidal wing was utilized with the nacelle-afterbody model of reference 1, to simulate the aft portion of a large wing for a supersonic cruise aircraft.

The investigation was conducted in the Lewis 8- by 6-foot supersonic wind tunnel with various 10.16-centimeter-diameter-nacelle-afterbody models. These models consisted of three 15°-conical boattails with a jet-to-nacelle-diameter ratio of 0.67. The radius of curvature at the afterbody juncture with the cylindrical nacelle was varied. The trapezoidal wing was designed with a relatively small planform area (approx 1900 cm^2) to avoid tunnel-blockage effects and excessive support loads and was mounted directly on the nacelle. The afterbodies were tested with the afterbody extending varying amounts downstream of the wing trailing edge. The conical forebody of the nacelle was closed, and the jet was simulated with a solid cylinder which had a diameter equal to the afterbody-base diameter. Data were obtained over a Mach number range from 0.56 to 1.00 at angles of attack from 0° to 6°. The Reynolds number based on nacelle diameter ranged from 1.20×10^6 to 1.50×10^6.

SYMBOLS

A area

C_a axial-force coefficient, (axial force)/$q_0 A_M$

C_p pressure coefficient, $(p - p_0)/q_0$

D diameter

L length from afterbody base to wing trailing edge

M Mach number

P total pressure

p static pressure

q dynamic pressure

R boattail-juncture radius of curvature

V velocity

x axial distance aft of nacelle-afterbody interface

x_M axial distance aft of forebody shoulder

y radial distance from model surface

α model angle of attack

β boattail trailing edge angle

δ boundary-layer thickness

Subscripts:

a axial

e nozzle-exit conditions

L local

M model nacelle

0 free-stream conditions

β boattail surface

APPARATUS AND PROCEDURE

The complete afterbody model configuration with the simulated wing, as installed in the Lewis 8- by 6-foot supersonic wind tunnel, is shown in figure 1. The basic model was a sting-supported, 10.16-centimeter-diameter-cylindrical section with a 10°-half-angle-conical forebody. Figure 2 is a sketch of the model installation showing the location of the model in the modified 8-foot, 3.1-percent porosity test section (see ref. 4). The tunnel station is the distance downstream of the beginning of the test section; the model nose was placed at tunnel station 0.0. Model blockage was 0.21 percent at 0° angle of attack.

Figure 3 illustrates the design of the wing simulator used for the afterbody tests. The airfoil section used for the wing simulator was a simple trapezoid, as shown in the sketch, with a maximum thickness of 2.025 percent. A thin section was used to avoid

flow separation on the upper surface of the wing at angle of attack. The incidence angle between the cylindrical section of the nacelle and the wing lower surface was zero. The surface of the cylindrical section was tangent to the lower surface of the wing simulator. The wing was translated longitudinally to obtain variations in the nozzle-extension ratio. The nozzle-extension ratio is defined as the distance from the afterbody base to the wing trailing edge ratioed to the nacelle diameter. Nozzle-extension ratios of 0.866, 1.116, and 1.366 were investigated. Although the wing simulator had a small aspect ratio, it is felt the flow in the region of the afterbody was essentially two-dimensional since the nacelle diameter was relatively small compared to the wing span.

The boattails were tested in the presence of a jet simulator extending aft from the afterbody base. The purpose of the simulator was to approximate the local flow field that would exist if a jet were present with an exit-to-local-static-pressure ratio of 1.0. Details of the jet simulator are shown in figure 4. It was shown in reference 1 that the boattail-drag data obtained with a jet simulator at subsonic Mach numbers were in good agreement with cold-jet data interpolated for values of $p_e/p_0 = 1.0$.

The afterbody geometries which were investigated are shown in figure 5. The afterbody geometries included a cylindrical afterbody with boundary-layer rakes and three 15°-conical boattails with radii of curvature of 0-, 0.5-, and 1.0-nacelle diameters at the juncture with the cylindrical nacelle. The 15° boattails had a ratio of base to nacelle diameter of 0.67. The two boundary-layer rakes on the cylindrical afterbody were located 6.48 centimeters aft of the nacelle-afterbody interface. This position coincides with the location of the boattail juncture of the $R/D_M = 0$ boattail. On boattails with radii of curvature, the curvature was tangent to both the cylindrical and conical portions of the afterbody. Since the ratio of base diameter to nacelle diameter was held constant, increasing the radius of curvature increased the length of the boattail.

Details of the boundary-layer rakes are shown in figure 6. The top rake measured a boundary layer that had been modified by the wing while the bottom rake was relatively interference free. The total pressures from the rakes were used with local static pressures to compute values of V/V_0 using the Rayleigh-pitot equation.

Since the boattail axial-force coefficients were determined from boattail-pressure measurements, extensive pressure instrumentation was located on the afterbodies. Instrumentation details for the 15°, $R/D_M = 0$ boattail are shown in figure 7. Instrumentation of all afterbody configurations was similar. The axial projection of the boattail was divided into ten equal annular areas. Pressure taps were located around 180° of the centroid line of each annular area at 30° intervals. It was assumed that the local flow field would be symmetrical about the vertical centerline, so pressures were located only on one side of the boattail. Additional pressure taps were located near the corner of the boattails to help define boattail pressure distribution. These pressures were not used for drag determination. By instrumenting the boattail in this manner, an area-weighted

average of pressure coefficient can be computed. This average pressure coefficient is then used to compute the axial-force coefficient. The boattail axial-force coefficient computed in this manner does not include the afterbody-base drag or afterbody-skin-friction drag but pertains only to pressure forces acting on the boattail surface.

RESULTS AND DISCUSSION

Figure 8 shows the effect of the wing simulator on the pressure distribution along the nacelle surface 90° from the vertical centerline. Data are shown for the cylindrical afterbody at 0° angle of attack with an extension ratio of 0.866. In general, the presence of the wing simulator reduced the local pressure in the region underneath the wing and increased pressure levels on the afterbody surface aft of the wing trailing edge compared to an isolated nacelle.

The effect of the wing simulator on the nacelle pressure distribution with nozzle-extension ratios of 1.116 and 1.366 is shown in figure 9. Data are shown only for the cylindrical portion of the nacelle ahead of the afterbody-nacelle interface. In general, the effect of the wing simulator is the same in that overall pressure levels are reduced in the region underneath the wing surface. Translating the wing leading edge with respect to the model shoulder seems to have little effect on model pressure distribution.

Boattail pressure distributions with a simulated wing and with an extension ratio of 0.866 are presented in figures 10, 11, and 12 for boattails with radii of curvature of 0-, 0.5-, and 1.0-model diameters, respectively. Figures 13 and 14 present pressure distributions for a boattail with a radius ratio of 0.5 at nozzle-extension ratios of 1.116 and 1.366. Data are shown over a range of Mach numbers at various angles of attack. Distributions are shown for rows along the top, side, and bottom of the boattail. The zero-angle-of-attack-pressure distributions of the isolated boattails from reference 1 are also shown for comparison. In general, the pressures on the isolated boattails at 0° angle of attack are lower than on the boattails with the wing simulator present. The boattails under the influence of the simulated wing, at the nozzle-extension ratios investigated, showed little effect of angle of attack on the circumferential pressure distribution, especially when compared to the effects observed on the isolated boattails in reference 1.

The effect of the wing-simulator flow field on the boattail-axial-force coefficients are shown in figure 15. Data for boattails with a simulated wing at an extension ratio of 0.866 are compared to isolated data from reference 1 for boattail-radius ratios of 0, 0.5, and 1.0 at various angles of attack. The presence of the simulated-wing flow field decreases the axial-force coefficient over the entire range of variables tested. The presence of the wing also modifies the shape of the drag curves so that the drag curve is reflexed between Mach numbers 0.75 and 0.85. This effect becomes more pronounced as

the radius of curvature is increased. At Mach 0.9, with 0° angle of attack, the wing reduces the axial-force coefficient 58, 71, and 88 percent for boattails with radius ratios of 0, 0.5, and 1.0, respectively. The presence of the simulated-wing flow field severely reduces the effect of angle of attack on axial-force coefficient, especially at the lower subsonic Mach numbers.

The effect of boattail radius of curvature on axial-force coefficients of boattails under the influence of a simulated wing with an extension ratio of 0.866 is shown in figure 16. Data are shown for boattail-radius ratios of 0, 0.5, and 1.0 at various angles of attack. At the lower subsonic Mach numbers (i.e., Mach 0.6 and 0.7), the boattail with a radius ratio of 0.5 results in the highest axial-force coefficient and the boattail with a radius ratio of 1.0 results in the lowest, although the overall effects of curvature in this Mach number range are relatively small. At all other Mach numbers tested, increasing the boattail radius of curvature decreased the boattail-axial-force coefficient for all angles of attack investigated. It was shown in reference 1 that increasing the radius ratio from 0 to 0.5 on an isolated boattail at 0° angle of attack resulted in a 44-percent reduction in boattail-axial-force coefficient at Mach 0.8 and a 27-percent reduction at Mach 0.9. The same boattails under the influence of the simulated wing at 0° angle of attack produced reductions in axial-force coefficient of 23 percent at Mach 0.8 and 50 percent at Mach 0.9. It is concluded, therefore, that the presence of the wing simulator decreases the effect of radius of curvature at Mach 0.8 and increases the effect at Mach 0.9.

Figure 17 shows the effect of nozzle-extension ratio on the axial-force coefficients of a boattail with a radius ratio of 0.5. Data are shown for angles of attack from 0° to 6°. Axial-force coefficients obtained with nozzle-extension ratios of 0.866, 1.116, and 1.366 are presented along with isolated data. In general, increasing the nozzle-extension ratio increases the boattail-axial-force coefficient, except at Mach 0.85, where increasing the extension ratio initially decreases the axial-force coefficient and then increases it. At Mach numbers 0.6, 0.7, and 0.8, increasing the extension ratio from 0.866 to 1.116 has very little effect on the axial-force coefficient; however, increasing the extension ratio from 1.116 to 1.366 at the same Mach numbers increases the boattail-axial-force coefficient considerably at all angles of attack investigated. The isolated data are presented because, ideally, increasing the nozzle-extension ratio to infinity would result in axial-force coefficients corresponding to isolated data.

The effect of the simulated wing on the afterbody boundary layer is shown in figure 18. Two boundary-layer rakes were located on the vertical centerline of the cylindrical afterbody; one was located on the top, behind the wing trailing edge, and the other was located 180° away. The boundary-layer survey plane was located 6.48 centimeters aft of the afterbody-nacelle interface. Data are presented for a range of Mach numbers for both top and bottom rakes. The nozzle-extension ratio is 0.866. It is felt the bottom rake represents reasonably well the boundary layer that would exist in the afterbody re-

gion if the wing were not present. Although the wing has little or no effect on boundary-layer thickness and profile, it does create a slight local velocity decrement for all the data shown. This effect is most pronounced at Mach 0.9. It is recognized that the simulated wing was not capable of producing the thick boundary layers that would exist with a complete wing. This boundary-layer effect may be very significant but is beyond the scope of the present study.

SUMMARY OF RESULTS

A 10.16-centimeter-diameter-cylindrical-nacelle model was tested in the Lewis 8- by 6-foot supersonic wind tunnel with 15°-conical boattails having radii of curvature of 0-, 0.5-, and 1.0-nacelle diameters at their juncture with the nacelle. The afterbodies were tested with the nozzle exit extended 0.866-, 1.116-, and 1.366-nacelle diameters downstream of a small trapezoidal-wing trailing edge. The conical nose of the nacelle was closed, and the jet was simulated with a cylindrical surface. Data were obtained over a Mach number range from 0.56 to 1.00 and angles of attack from 0° to 6°. The following observations were made:

1. The presence of the simulated-wing flow field reduced the axial-force coefficients from the isolated values over the entire range of variables tested. At Mach 0.9, for example, the wing reduced the boattail-axial-force coefficients 58, 71, and 88 percent for boattails with radii of curvature of 0-, 0.5-, and 1.0-model diameters at 0° angle of attack and an extension ratio of 0.866.

2. The presence of the simulated-wing flow field reduced the effects of angle of attack, especially at the lower subsonic Mach numbers.

3. In general, increasing the boattail radius of curvature decreases the axial-force coefficient for afterbodies under the influence of a simulated wing. For example, increasing the radius of curvature from 0- to 0.5-model diameters reduced the axial-force coefficient 23 percent at Mach 0.8 and 50 percent at Mach 0.9.

4. In general, increasing the nozzle-extension ratio increases the boattail-axial-force coefficient, except at Mach 0.85 where increasing the extension ratio initially decreases the boattail-axial-force coefficient and then increases it.

Lewis Research Center,
National Aeronautics and Space Administration,
Cleveland, Ohio, April 26, 1968,
126-15-02-10-22.

REFERENCES

1. Shrewsbury, George D.: Effect of Boattail Juncture Shape on the Pressure Drag Coefficients of Isolated Afterbodies. NASA TM X-1517, 1968.

2. Silhan, Frank V.; and Cubbage, James M., Jr.: Drag of Conical and Circular-Arc Boattail Afterbodies at Mach Numbers From 0.6 to 1.3. NACA RM L56K22, 1957.

3. Pel, C.; and Rustmeyer, A.: Investigation of Turbojet Exhaust-Interference Drag. Rep. No. R-0801-12, United Aircraft Corp., Nov. 1955.

4. Mitchell, Glenn A.: Effect of Model Forebody Shape on Perforated Tunnel Wall Interference. NASA TM X-1656, 1968.

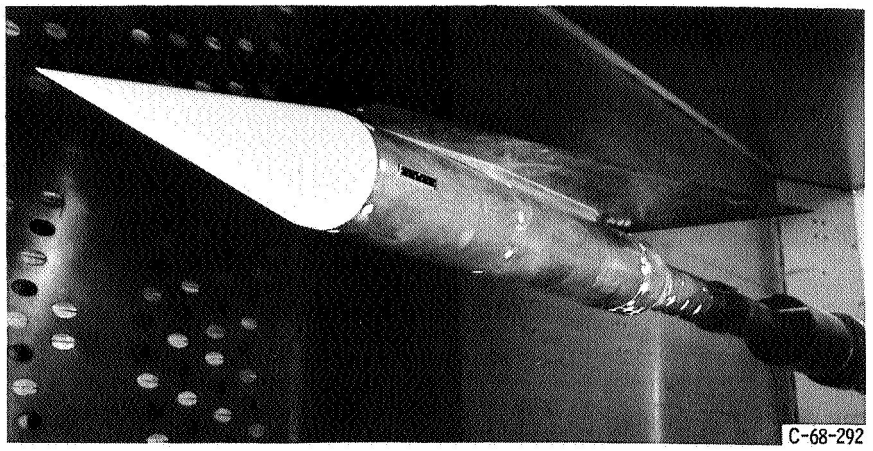

Figure 1. - Afterbody model installed in 8- by 6-foot supersonic wind tunnel.

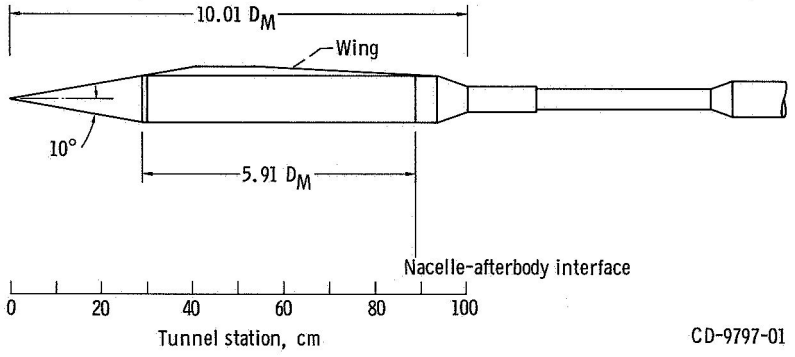

Figure 2. - Schematic of model assembly. Model diameter, D_M, 10.16 centimeters.

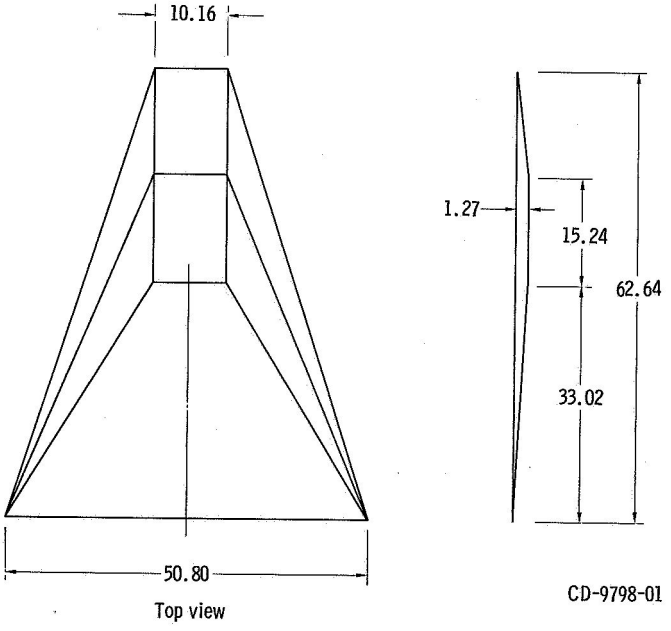

Figure 3. - Design of wing simulator. (All dimensions in centimeters.)

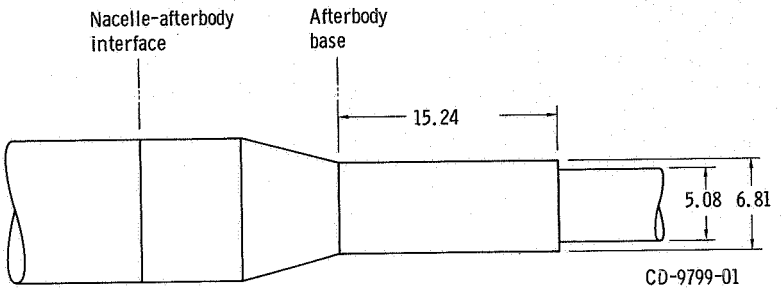

Figure 4. - Base geometry details showing sting and jet simulator. (All dimensions in centimeters.)

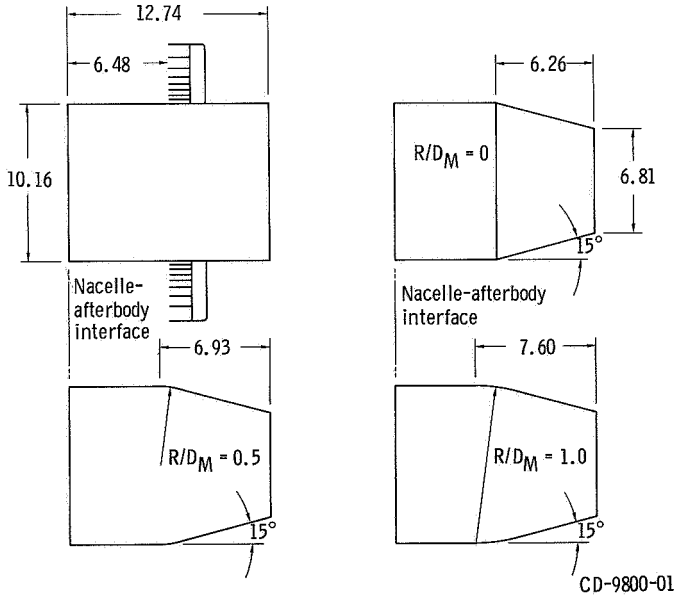

Figure 5. - Afterbody geometry details. (All dimensions in centimeters.)

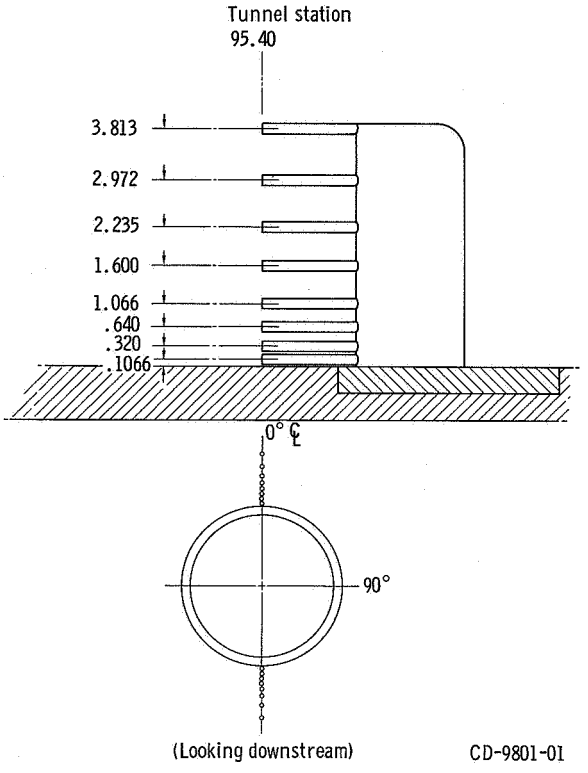

Figure 6. - Boundary layer rake details. (All dimensions in centimeters.)

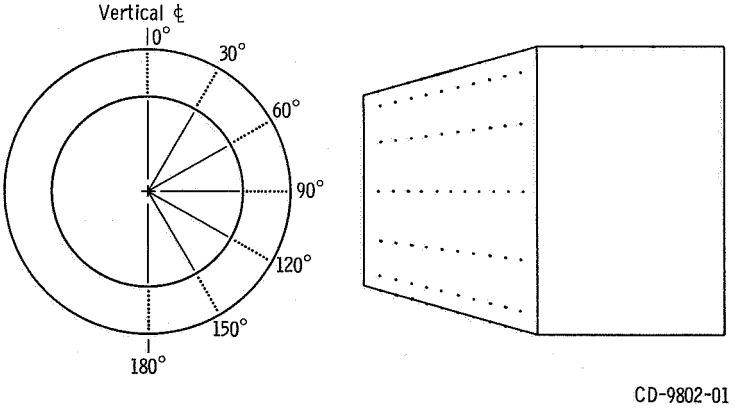

Figure 7. - Afterbody instrumentation details.

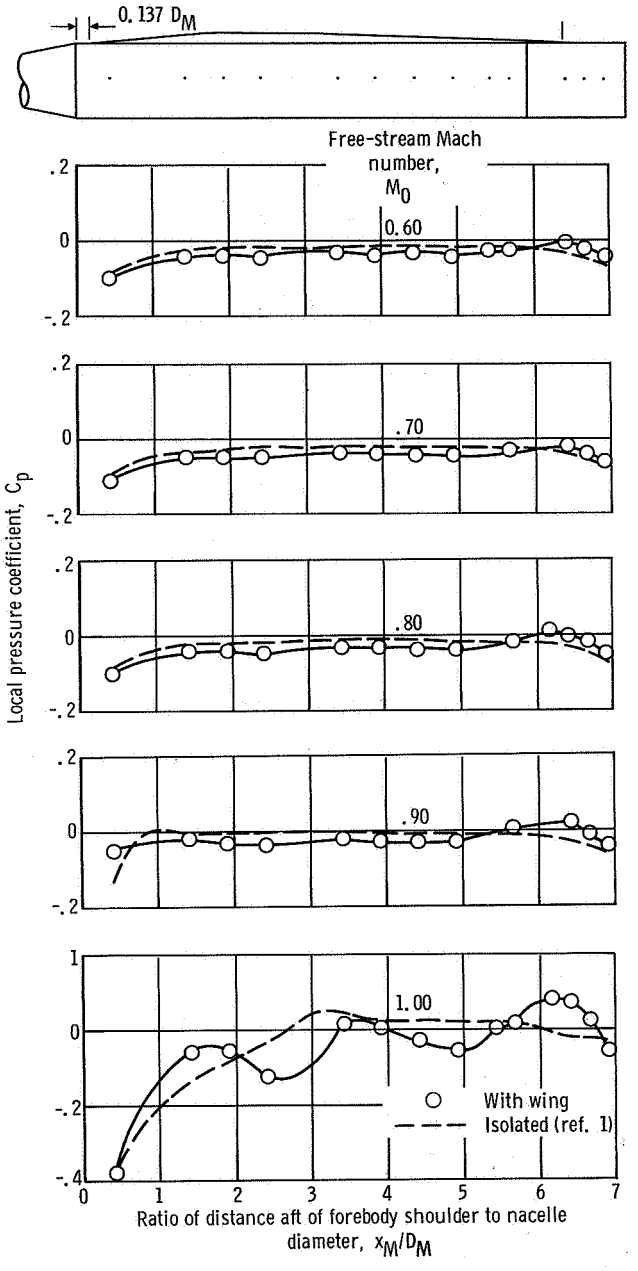

Figure 8. - Pressure distributions along nacelle, 90° from vertical centerline. Cylindrical afterbody; model angle of attack, 0°; nozzle extension ratio, 0.866.

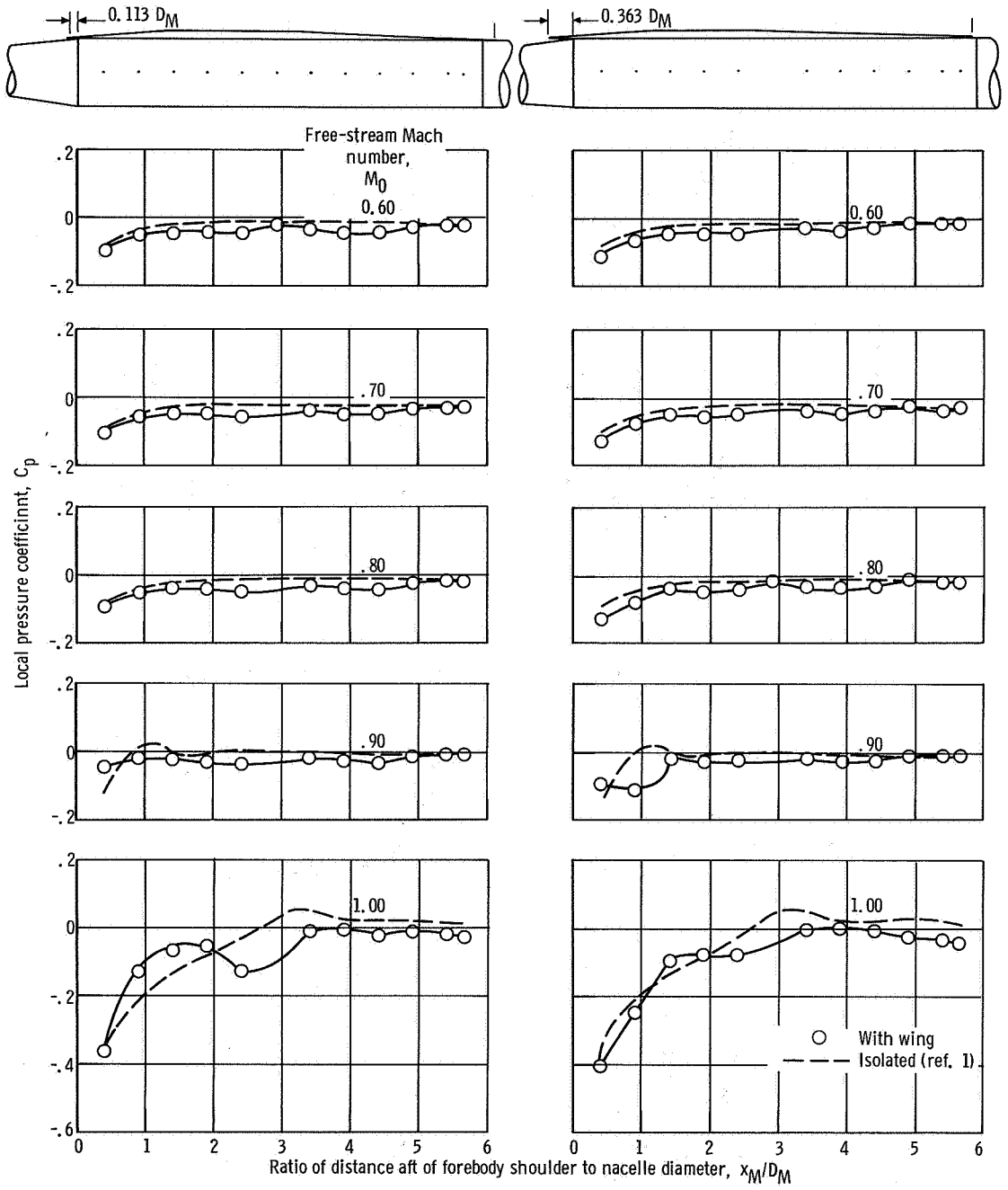

(a) Nozzle extension ratio, 1.116.

(b) Nozzle extension ratio, 1.366.

Figure 9. - Pressure distribution along nacelle, 90° from vertical centerline. Model angle of attack, 0°.

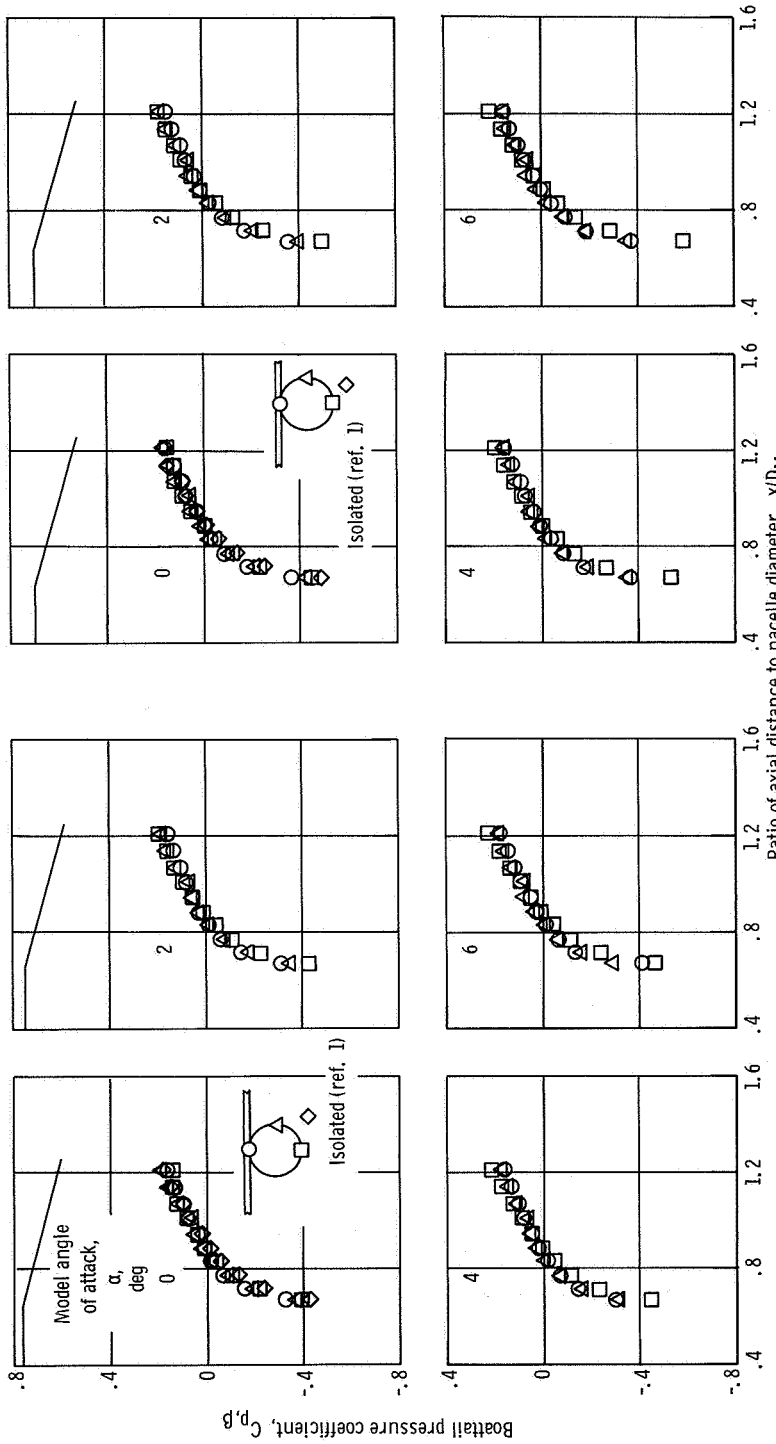

(a) Mach number, 0.60.

(b) Mach number, 0.70.

Figure 10. - Boattail pressure coefficient distribution. Boattail radius ratio, 0; nozzle extension ratio, 0.866.

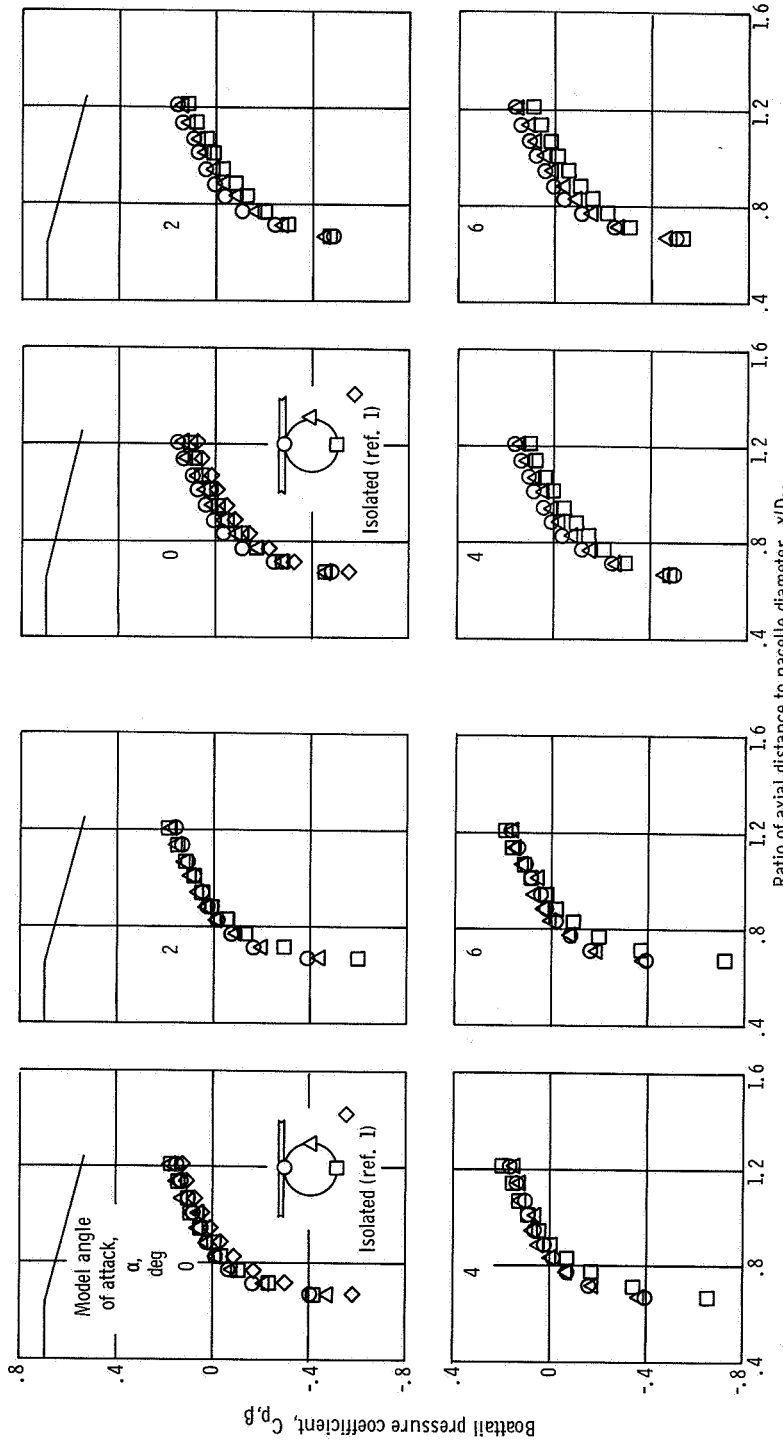

(c) Mach number, 0.80.

(d) Mach number, 0.90.

Figure 10. - Continued

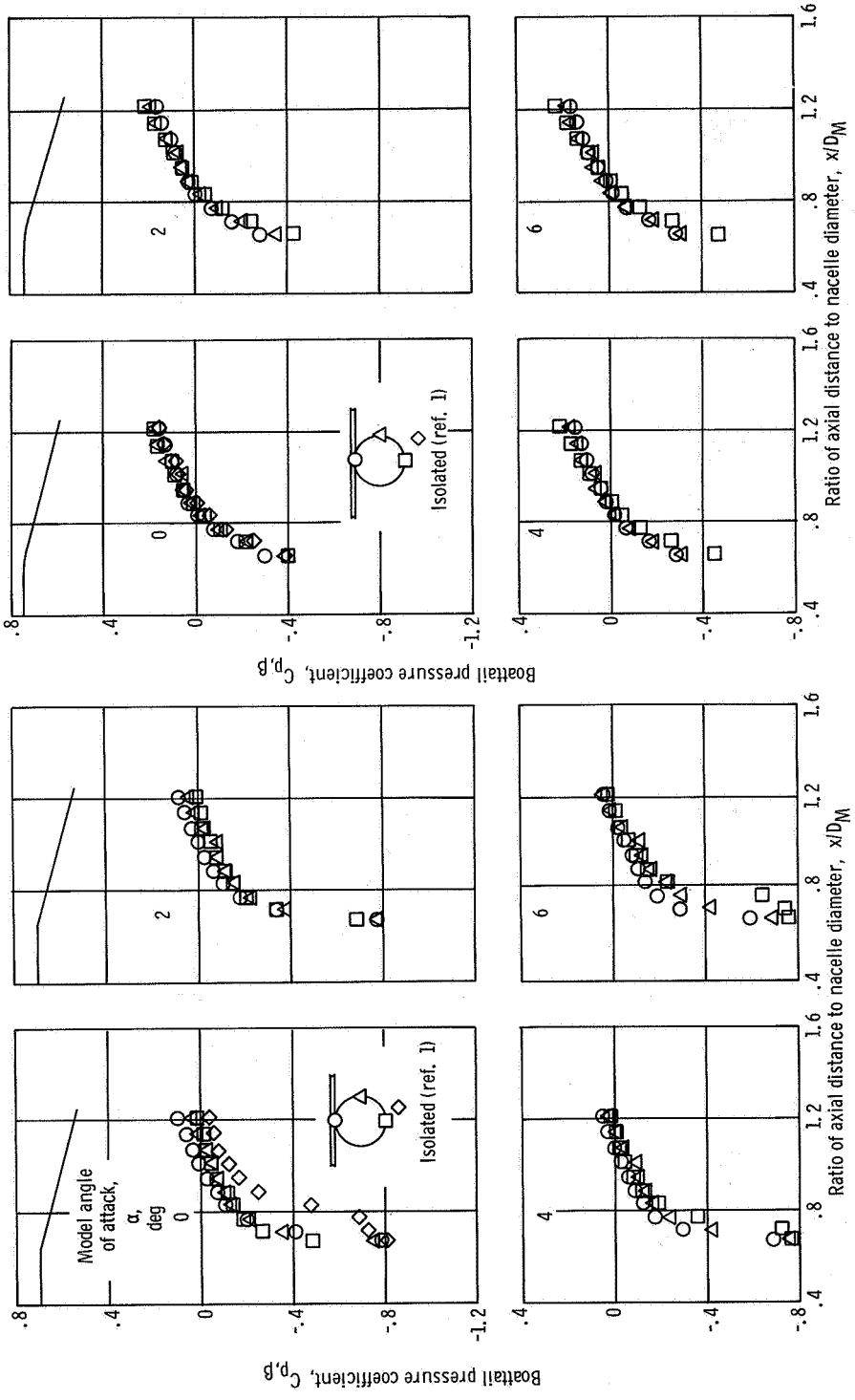

(a) Mach number, 0.60.

(e) Mach number, 1.00.

Figure 10. - Concluded.

Figure 11. - Boattail pressure coefficient distributions. Boattail radius ratio, 0.5; nozzle extension ratio, 0.866.

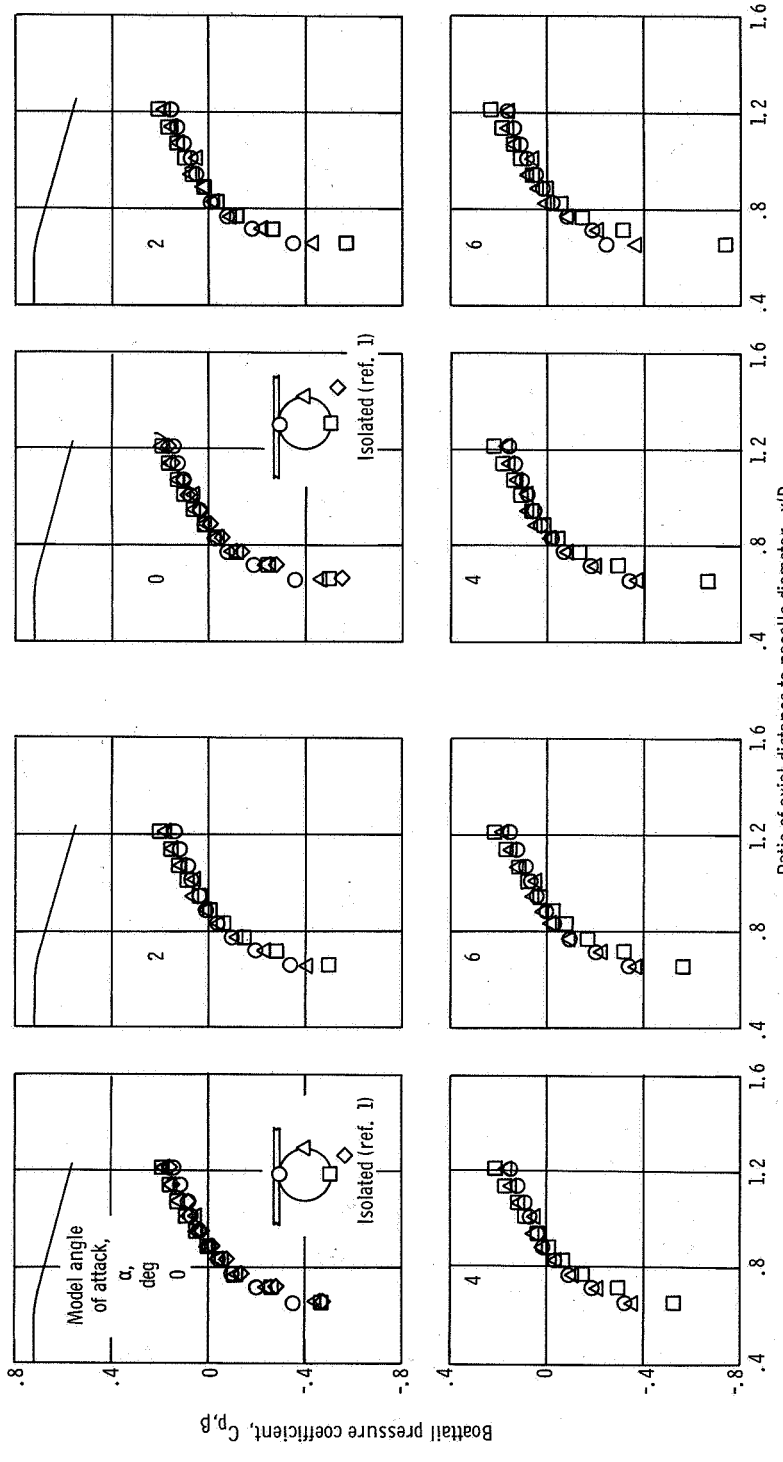

(b) Mach number, 0.70.

(c) Mach number, 0.80.

Figure 11. - Continued.

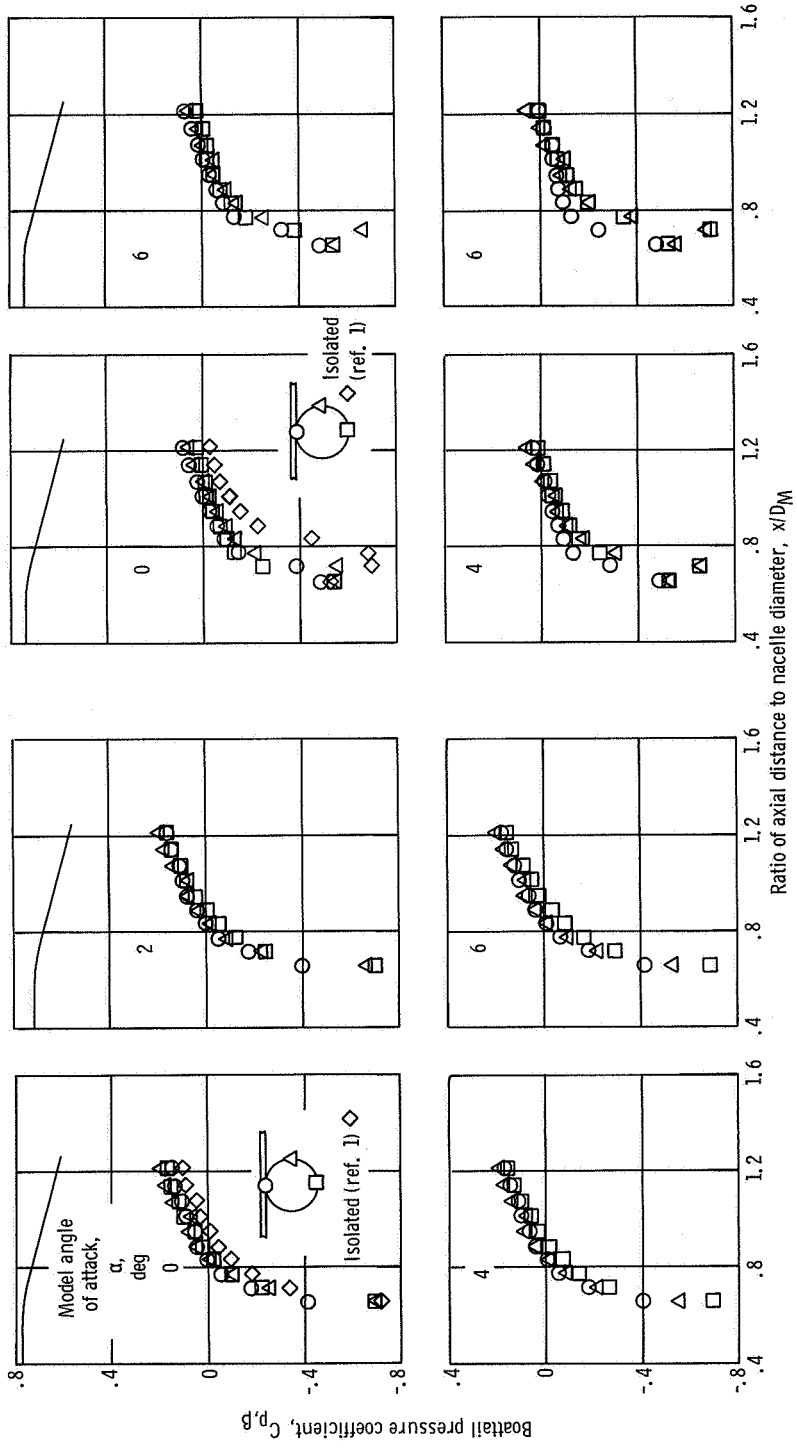

(d) Mach number, 0.90.

(e) Mach number, 1.00.

Figure 11. - Concluded.

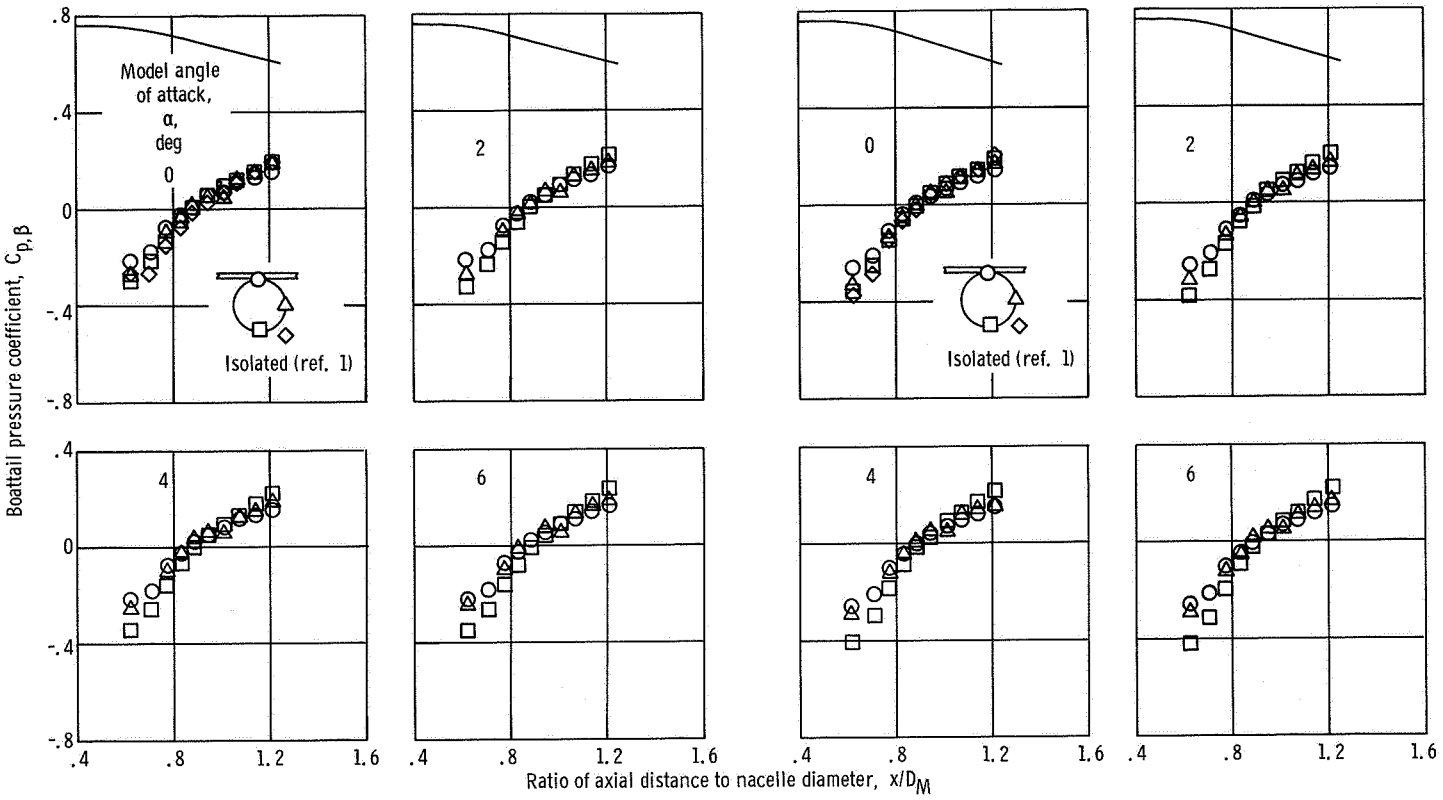

(a) Mach number, 0.60.

(b) Mach number, 0.70.

Figure 12. - Boattail pressure coefficient distributions. Boattail radius ratio, 1.0; wing extension ratio, 0.866.

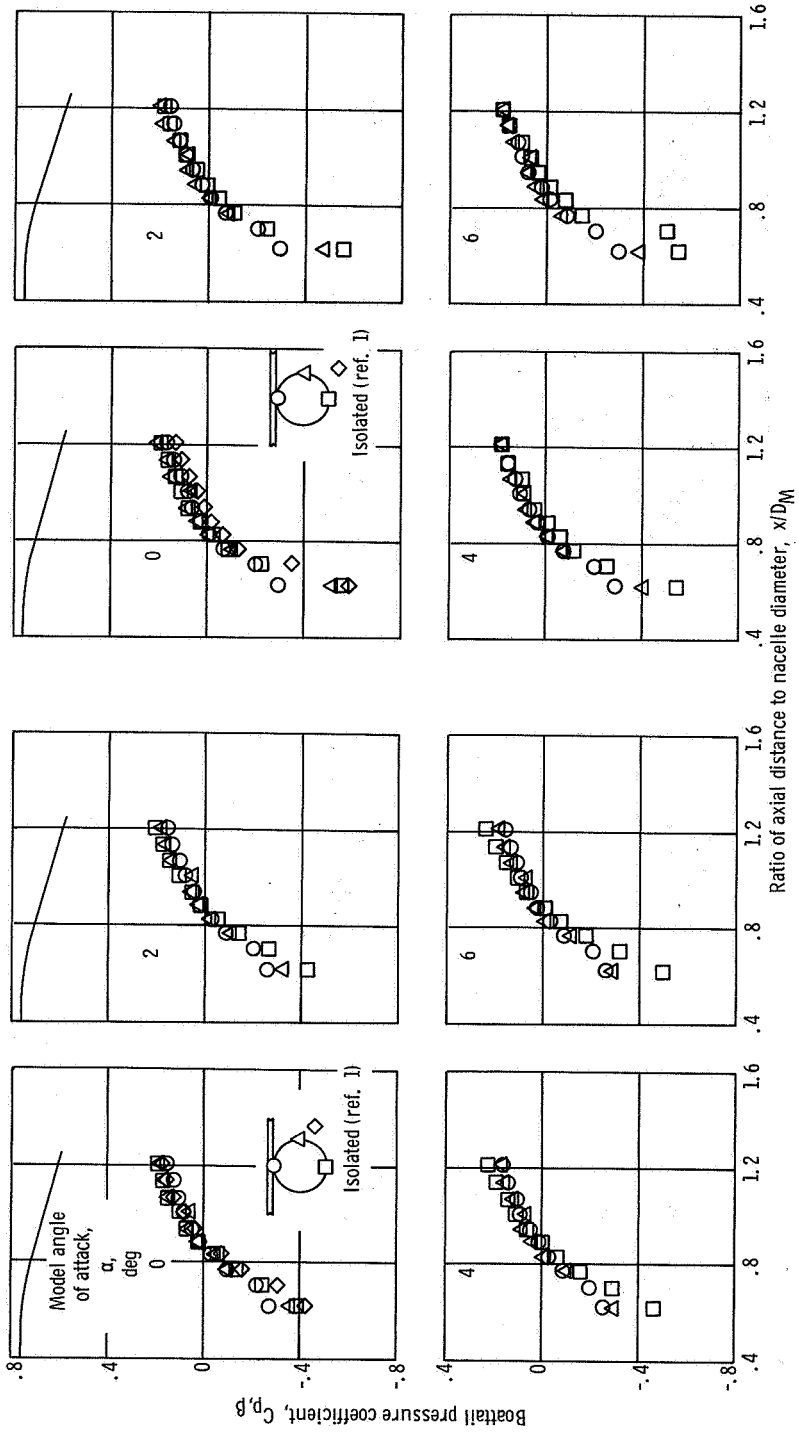

Figure 12. - Continued.

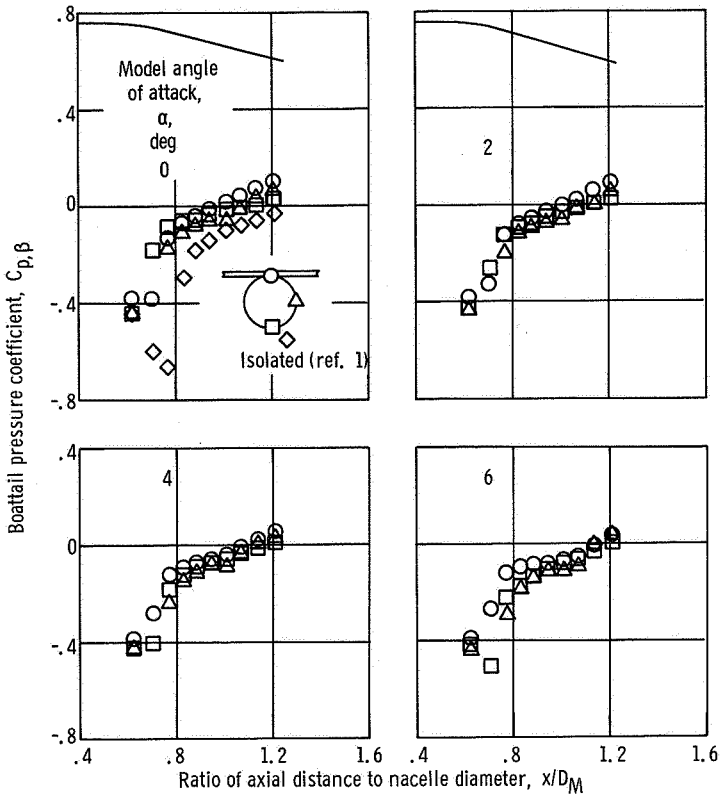

(e) Mach number, 1.00.

Figure 12. - Concluded.

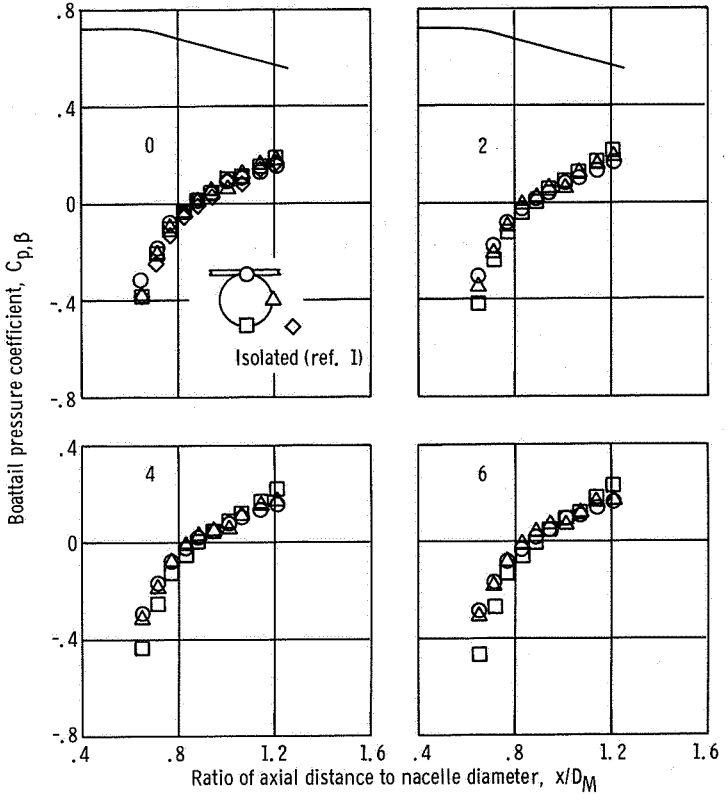

(a) Mach number, 0.60.

Figure 13. - Boattail pressure coefficient distributions. Boattail radius ratio, 0.5; nozzle extension ratio, 1.116.

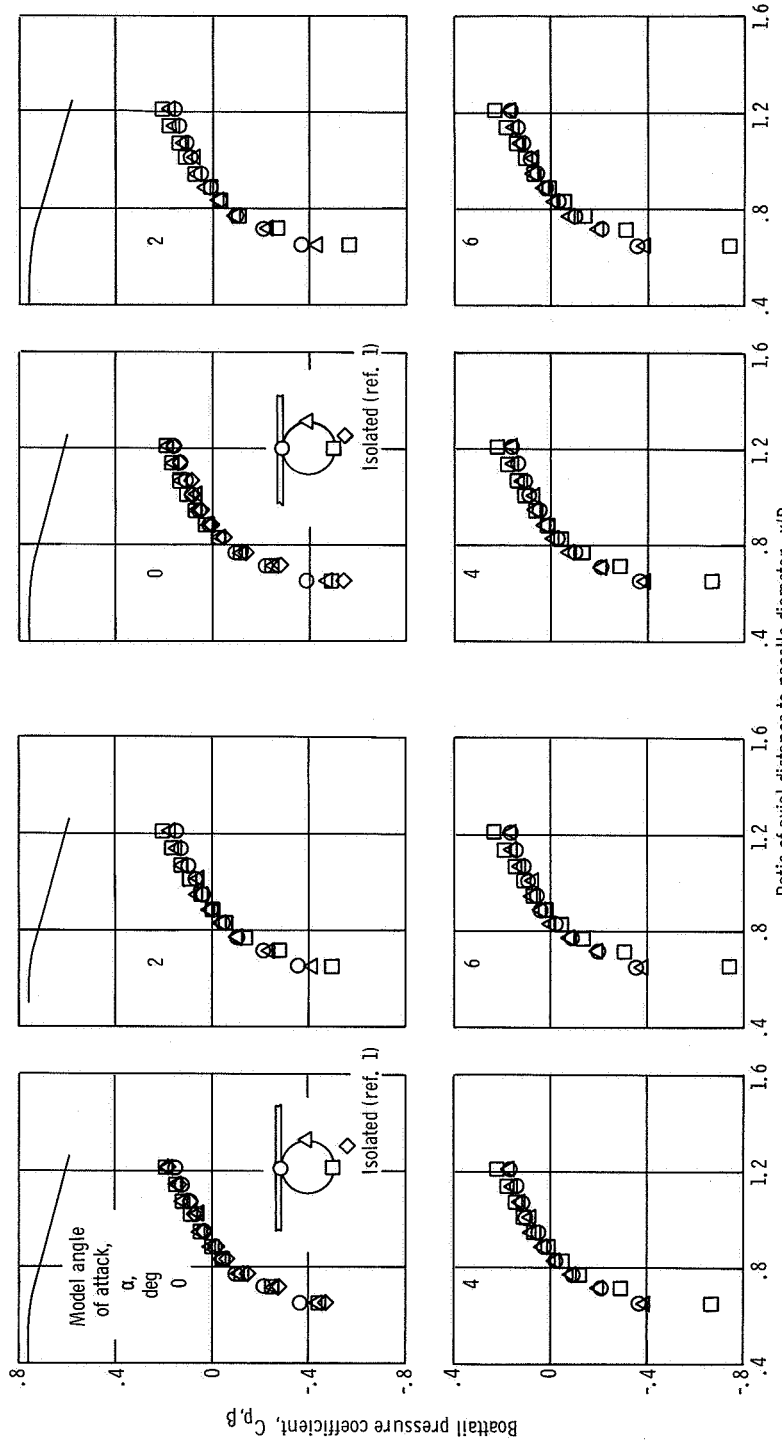

(b) Mach number, 0.70.

(c) Mach number, 0.80.

Figure 13. - Continued.

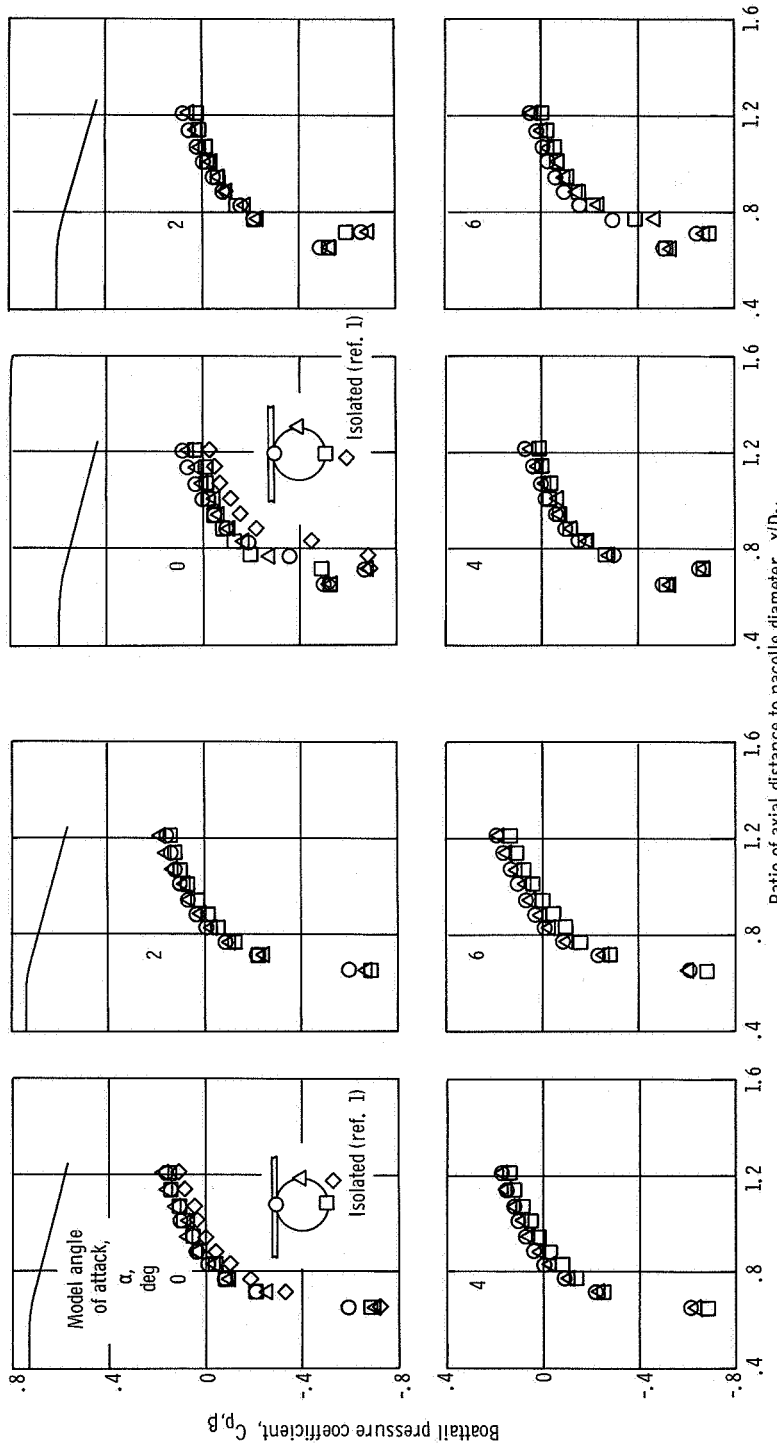

(d) Mach number, 0.90.

(e) Mach number, 1.00.

Figure 13. - Concluded.

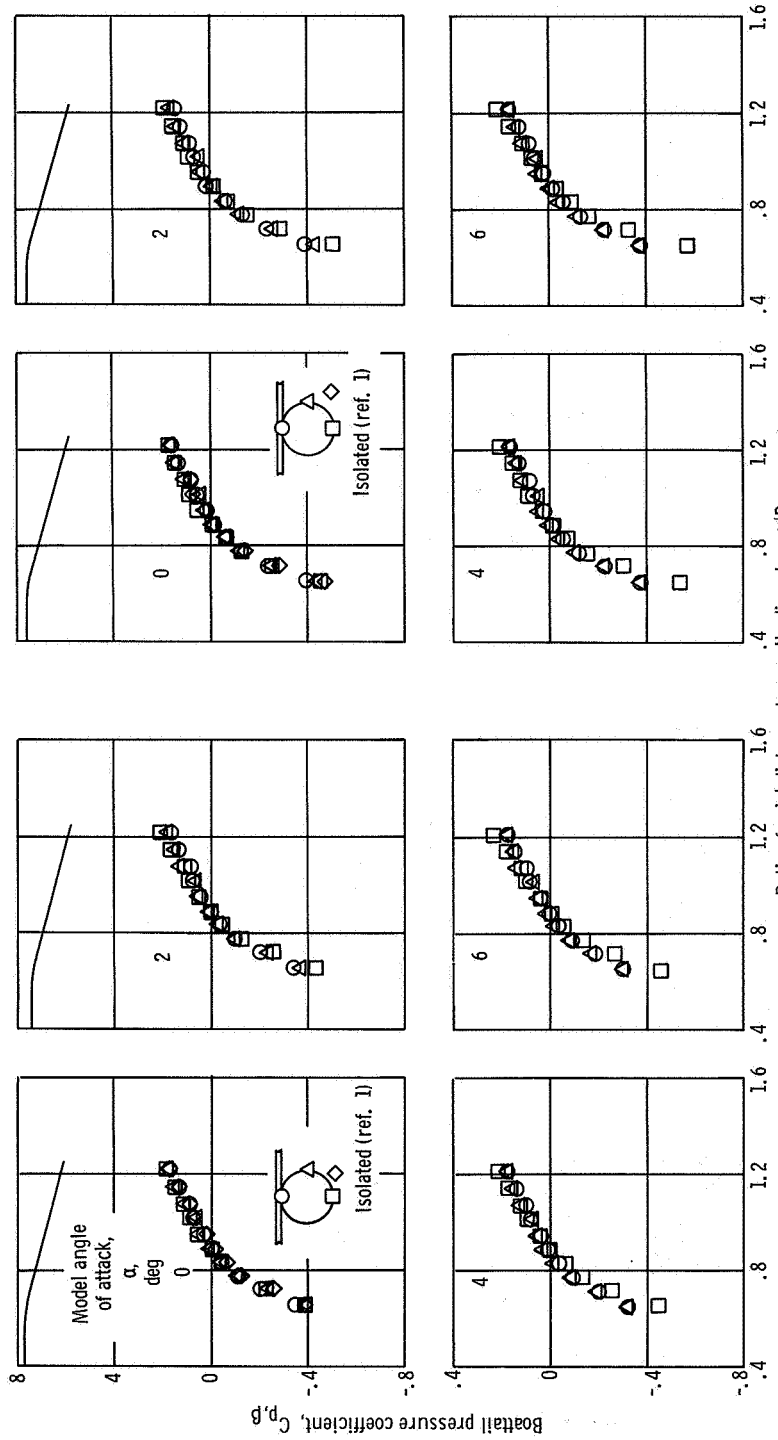

(a) Mach number, 0.60.

(b) Mach number, 0.70.

Figure 14. - Boattail pressure coefficient distributions. Boattail radius ratio, 0.50; extension ratio, 1.366.

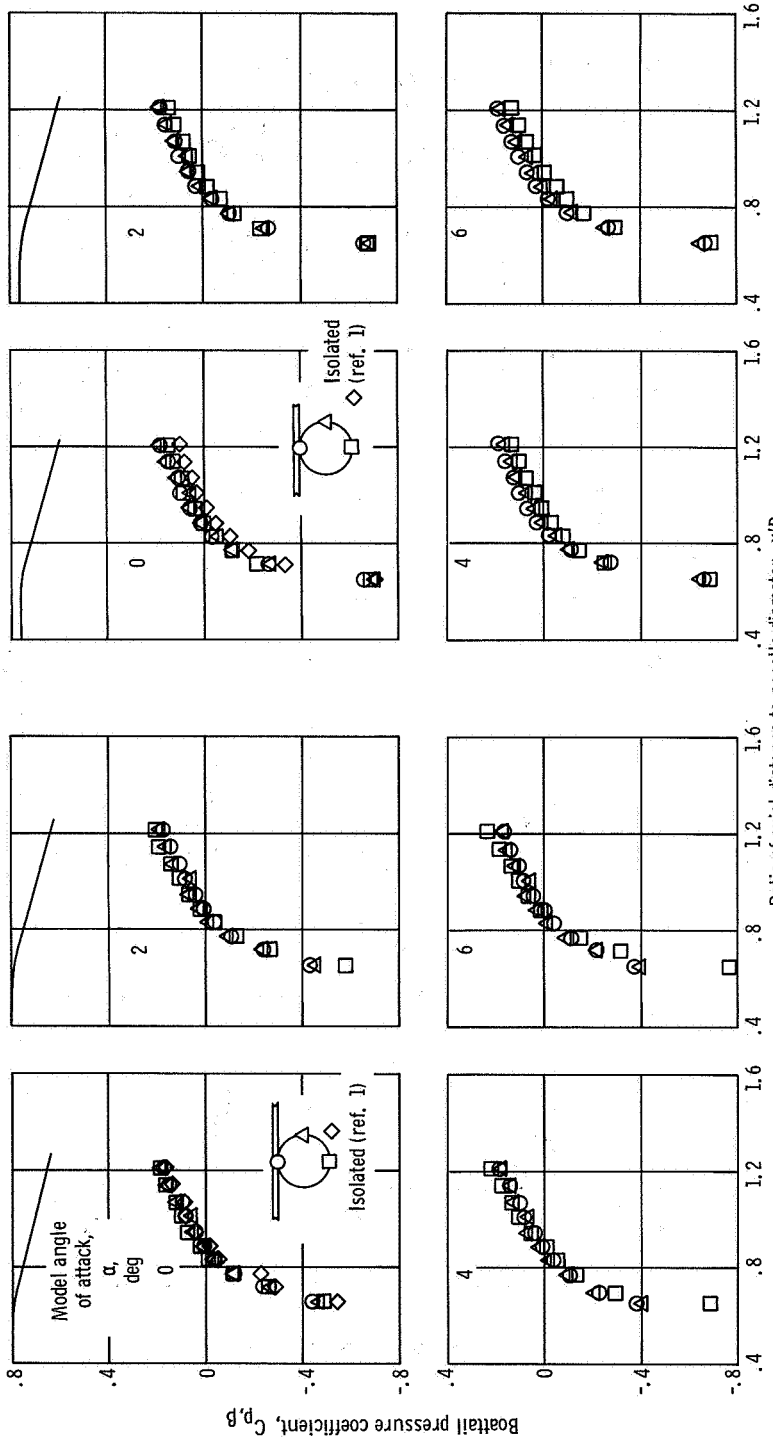

(c) Mach number, 0.80.

(d) Mach number, 0.90.

Figure 14. - Continued.

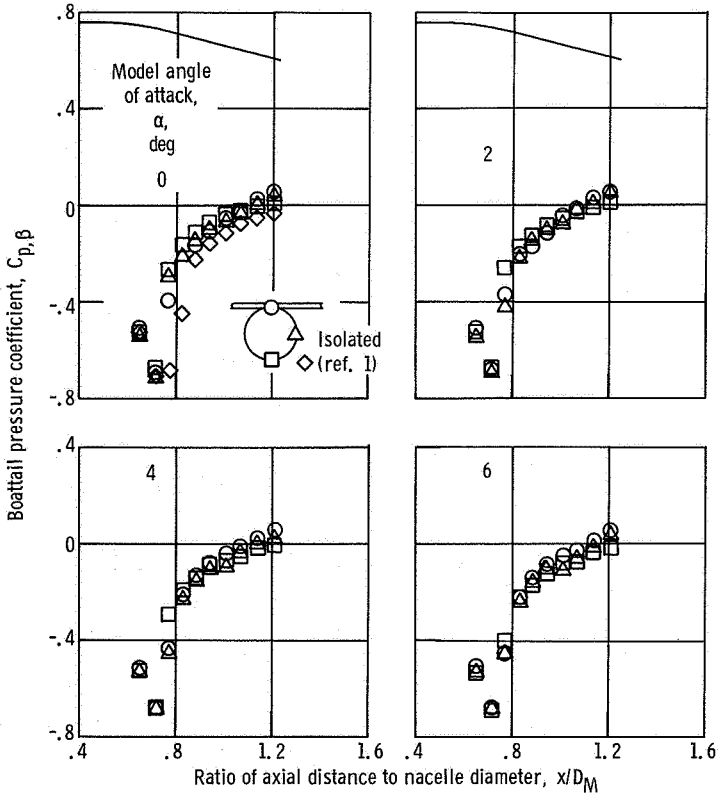

(e) Mach number, 1.00.

Figure 14. - Concluded.

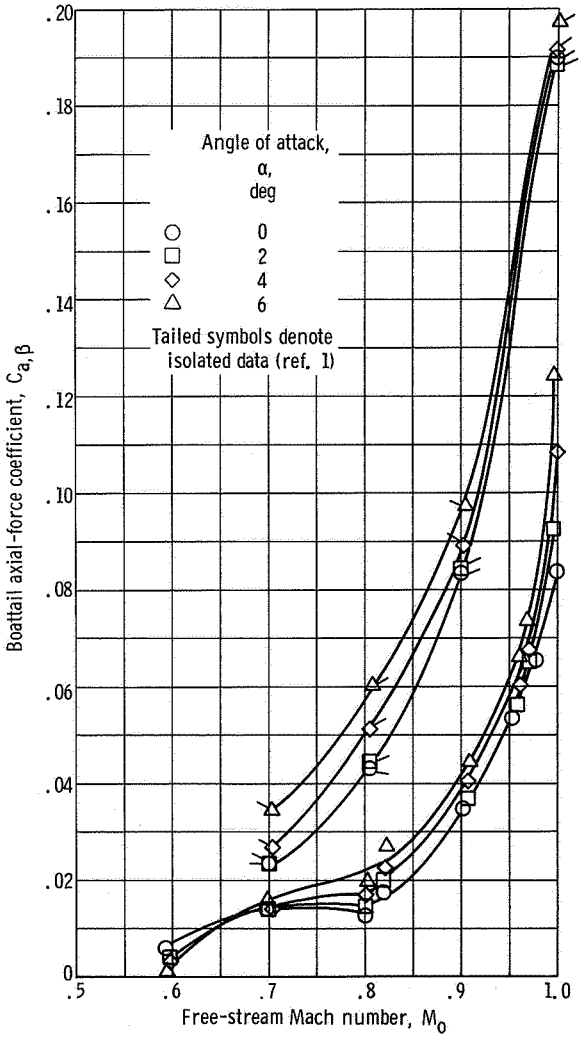

(a) Boattail radius ratio, 0.

Figure 15. - Effect of simulated wing flow field on boattail axial-force coefficients. Nozzle extension ratio, 0.866.

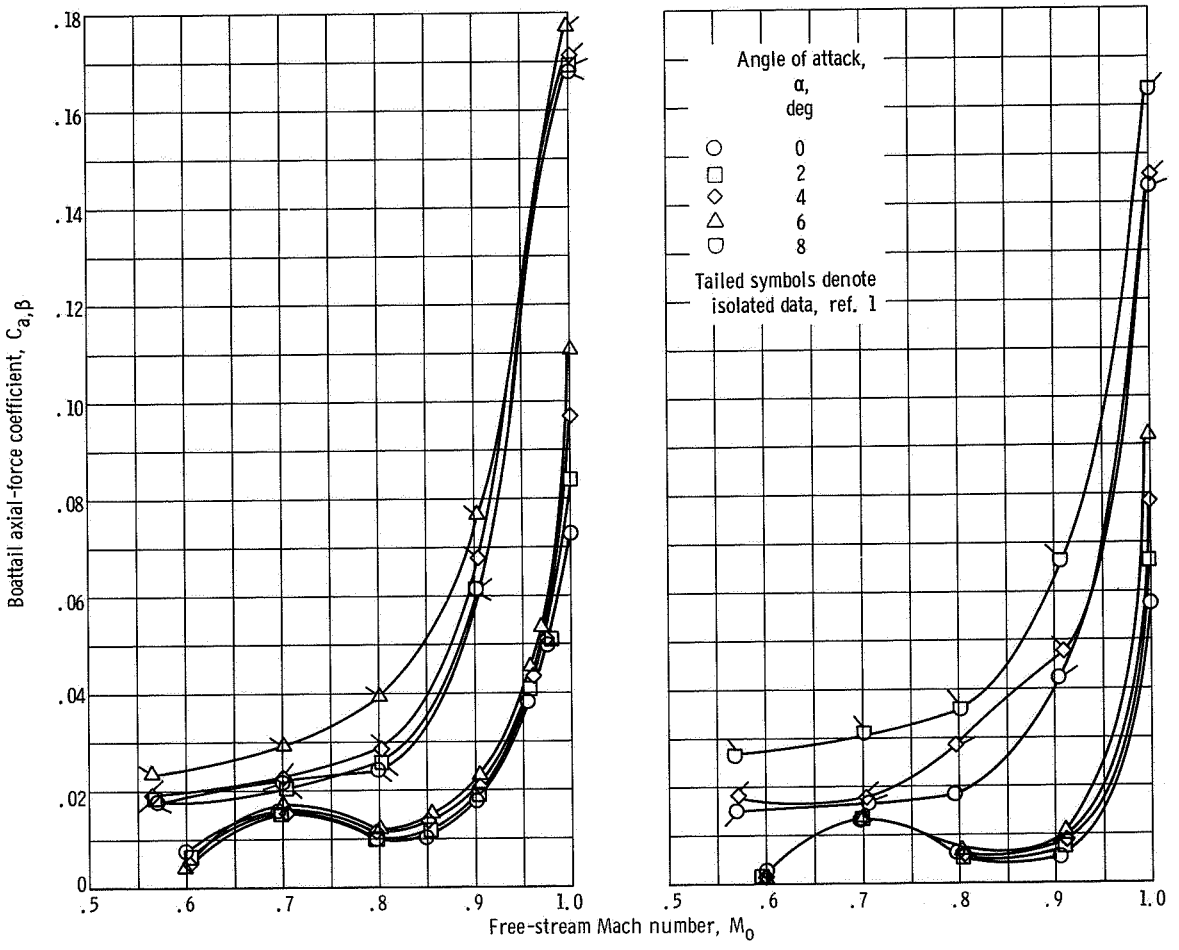

(b) Boattail radius ratio, 0.50.

(c) Boattail radius ratio, 1.0.

Figure 15. - Concluded.

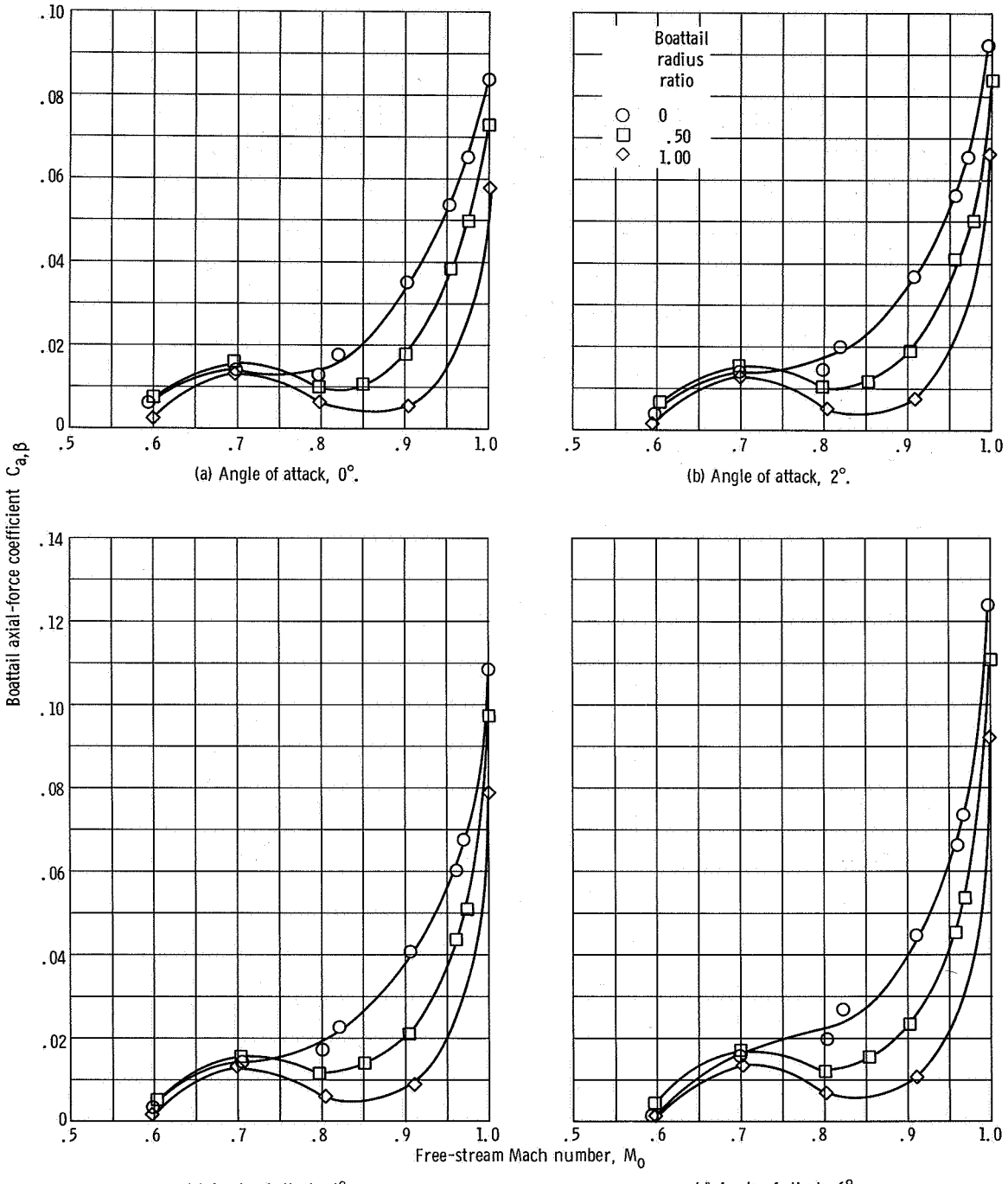

Figure 16. - Effect of boattail radius ratio on axial-force coefficients with simulated wing. Nozzle extension ratio, 0.866.

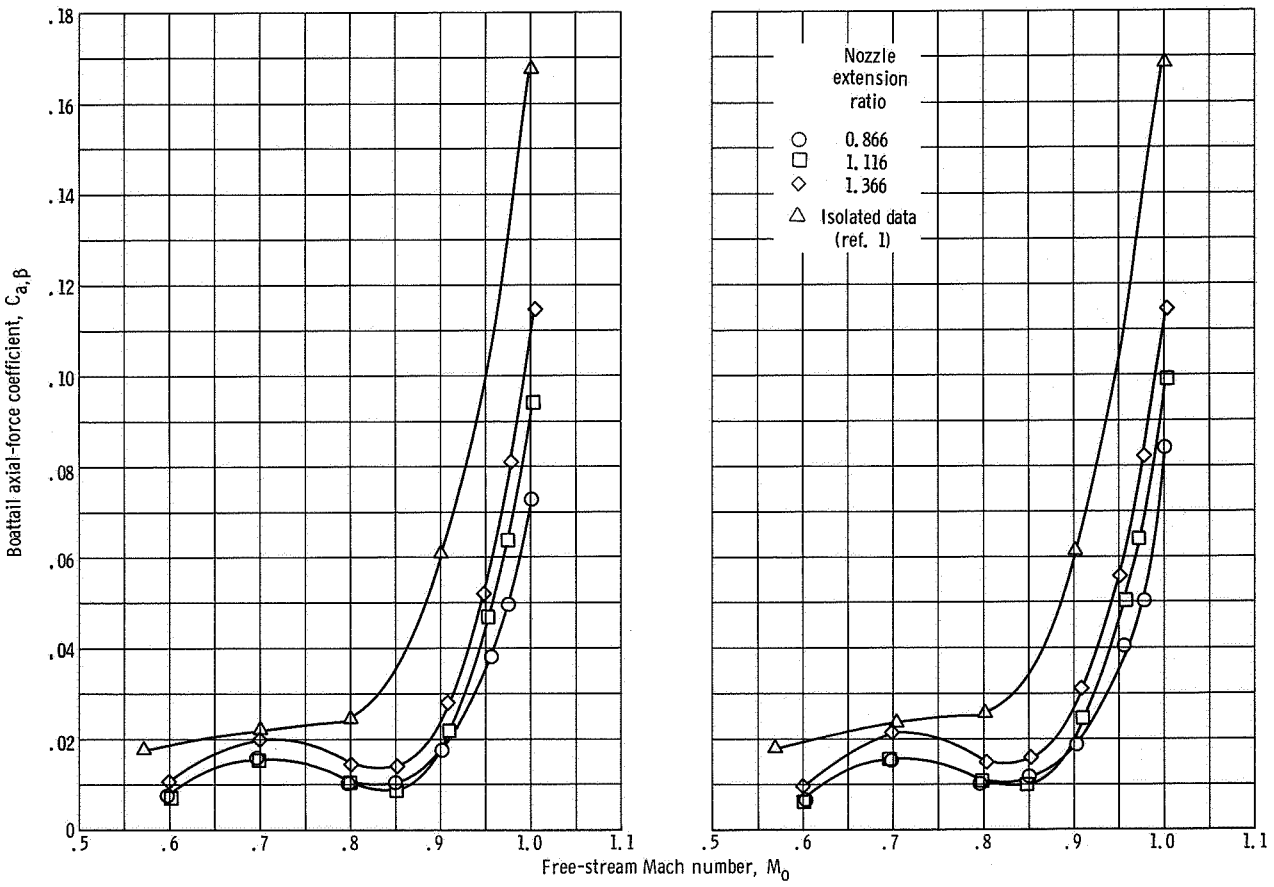

(a) Angle of attack, 0°.

(b) Angle of attack, 2°.

Figure 17. - Effect of nozzle extension ratio on boattail axial-force coefficient. Boattail radius ratio, 0.50.

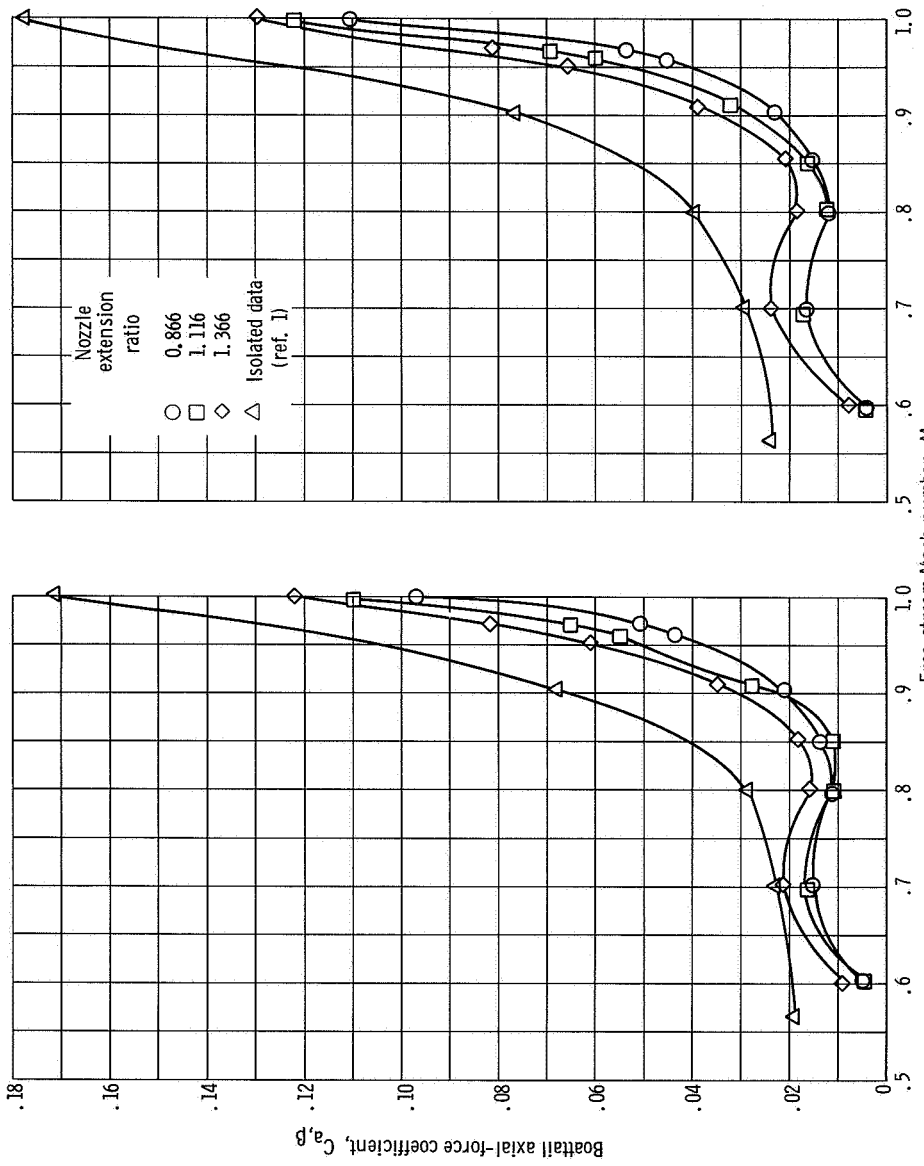

(c) Angle of attack, 4°.

(d) Angle of attack, 6°.

Figure 17. - Concluded.

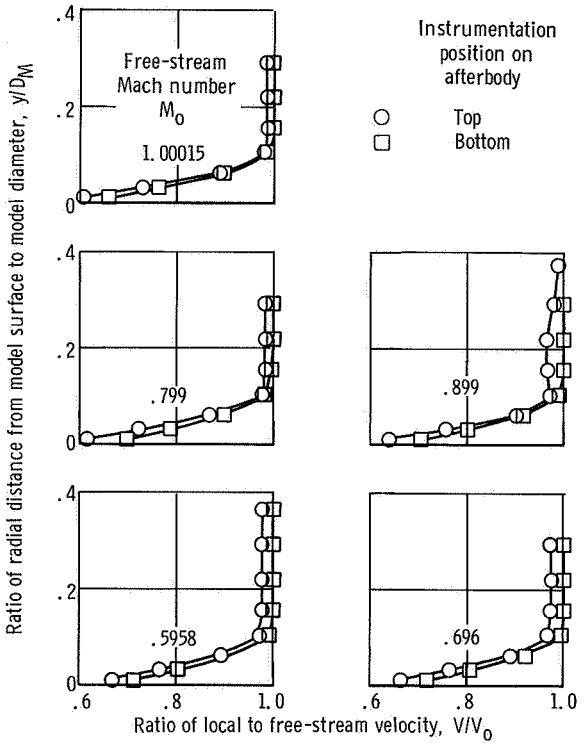

Figure 18. - Effect of simulated wing on afterbody boundary layer. Nozzle extension ratio, 0.866; angle of attack, 0°.

NATIONAL AERONAUTICS AND SPACE ADMINISTRATION
WASHINGTON, D.C. 20546

OFFICIAL BUSINESS

FIRST CLASS MAIL

POSTAGE AND FEES PAID
NATIONAL AERONAUTICS AND
SPACE ADMINISTRATION

POSTMASTER: If Undeliverable (Section 158
Postal Manual) Do Not Return

"The aeronautical and space activities of the United States shall be conducted so as to contribute . . . to the expansion of human knowledge of phenomena in the atmosphere and space. The Administration shall provide for the widest practicable and appropriate dissemination of information concerning its activities and the results thereof."

—NATIONAL AERONAUTICS AND SPACE ACT OF 1958

NASA SCIENTIFIC AND TECHNICAL PUBLICATIONS

TECHNICAL REPORTS: Scientific and technical information considered important, complete, and a lasting contribution to existing knowledge.

TECHNICAL NOTES: Information less broad in scope but nevertheless of importance as a contribution to existing knowledge.

TECHNICAL MEMORANDUMS: Information receiving limited distribution because of preliminary data, security classification, or other reasons.

CONTRACTOR REPORTS: Scientific and technical information generated under a NASA contract or grant and considered an important contribution to existing knowledge.

TECHNICAL TRANSLATIONS: Information published in a foreign language considered to merit NASA distribution in English.

SPECIAL PUBLICATIONS: Information derived from or of value to NASA activities. Publications include conference proceedings, monographs, data compilations, handbooks, sourcebooks, and special bibliographies.

TECHNOLOGY UTILIZATION PUBLICATIONS: Information on technology used by NASA that may be of particular interest in commercial and other non-aerospace applications. Publications include Tech Briefs, Technology Utilization Reports and Notes, and Technology Surveys.

Details on the availability of these publications may be obtained from:

SCIENTIFIC AND TECHNICAL INFORMATION DIVISION

NATIONAL AERONAUTICS AND SPACE ADMINISTRATION

Washington, D.C. 20546